Proceedings of FEDSM'98
1998 ASME Fluids Engineering Division Summer Meeting
June 21-25, 1998, Washington, DC

FEDSM98-5020

EFFECT OF SPATIAL RESOLUTION OF LES ON PARTICLE MOTION

Yasufumi Yamamoto, Toshitsugu Tanaka and Yutaka Tsuji
Department of Mechanical Engineering, Osaka University
2-1 Yamada-oka, Suita, Osaka,565, JAPAN
yamamoto@mupf., tanaka@, tsuji@ + mech.eng.osaka-u.ac.jp

ABSTRACT

Effects of spatial resolution of LES on particle trajectories have been studied. The trajectories calculated in high resolution LES were compared with those calculated in flow fields filtered by sharp cutoff filters. The relation between the Stokes number St and the eddy length scale λ was investigated by analyzing results obtained from numerical calculation as well as by a theoretical approach. In the present range of St, the theoretical prediction gives a good agreement with the numerical results qualitatively.

INTRODUCTION

The particle-turbulence interaction in gas-solid two-phase flows has two aspects, that is, the effects of particles on gas turbulence and the effect of turbulence on particle motion. These phenomena have been studied by many researchers. However our knowledge is not enough to predict the phenomena quantitatively. Since early 1990's, numerical simulations of two-phase turbulent flows have been performed by using the direct simulation techniques of turbulent flows (Squires & Eaton 1990, Elghobashi & Truesdell 1992). Regarding turbulent channel flows, Rouson & Eaton (1994) performed DNS and Wang & Squires (1996) performed LES. They showed that heavy particles tend to disperse uniformly and light particles tend to form clusters.

When considering the performance of present super computers, DNS is not suitable for gas-solid channel flows of interest because the range of Reynolds number is limited to low values compared with flows in practice. Thus, we decided to use LES. The authors have performed LES of particle-laden turbulent channel flow (Tanaka *et al.* 1997) which contains large-inertia particles in the same conditions as those of the experiments by Kulick *et al.* (1994) and Fessler *et al.* (1996). We have pointed out the effect of inter-particle collision on the dispersion of particles is very large even in a small solid volume fraction $O(10^{-4})$. When the particle Stokes number which is defined as the ratio of the particle relaxation time to the characteristic time of turbulence is large, the effect of sub-grid-scale (SGS) eddies on particle motion is negligible. However, the particle which has a small Stokes number should be affected by the SGS eddies. Therefore the effect of spatial resolution of LES on the particle motion must be studied when small-inertia particles are treated.

In this paper, the effect of spatial resolution of LES on the trajectories of particles was studied. Wang & Squires (1996) estimated the effect of SGS fluctuation velocity on the motion of light particles using the transport equation of SGS kinetic energy. However, models are required in the equation of SGS kinetic energy and in the process to transform SGS energy to SGS fluctuation velocity. We examined the effect of small eddies on the motion of particles by filtering the fluid flow field. The motions of particles were calculated simultaneously both in the raw flow field and in the filtered flow fields. The raw flow field means the one which is directly calculated by LES with high resolution grids. In the filtered flow fields small eddies in the raw flow fields are eliminated by applying the sharp cutoff filter to the gas velocity field. More than twenty filtered fields were provided by changing the cutoff wave number. The effect of the spatial resolution of LES was studied by comparing particle trajectories in the raw flow field with those in filtered flow fields. In addition the spatial resolution of LES which can resolve particle motion was examined.

LES OF TURBULENT CHANNEL FLOW

Figure 1 shows the calculation region. Downward flows were treated. Periodic boundary conditions were applied in the streamwise and spanwise directions. The Cartesian coordinate system was used. That is,

x or x_1 : streamwise direction,

y or x_2 : wall-normal direction,

z or x_3 : spanwise direction.

The filtered equations of continuity and momentum are as follows.

$$\frac{\partial u_i}{\partial x_i} = 0, \tag{1}$$

$$\left.\begin{aligned} &\frac{\partial u_i}{\partial t} = \frac{\partial F_{ij}}{\partial x_j} \\ &F_{ij} = -\delta_{ij}\frac{p}{\rho} - u_i u_j + 2\nu S_{ij} - \overline{u'_i u'_j}^{(SGS)} \end{aligned}\right\}, \tag{2}$$

where u_i, p are grid scale velocity and pressure. S_{ij} is strain rate tensor, $S_{ij} = (1/2)\left(\partial u_i/\partial x_j + \partial u_j/\partial x_i\right)$, and $\overline{u'_i u'_j}^{(SGS)}$ is SGS Reynolds stress. In our previous study we have pointed out that the effect of two-way coupling cannot be neglected even in a solid volume fraction $O(10^{-4})$. However, in the present study we focus our attention to the effect of spatial resolution of LES on the motion of particles, so we neglected the effect of particle on gas-phase flow (one-way coupling) for simplicity. As SGS model, we applied Smagorinsky model (Deardorff, 1970),

$$\left.\begin{aligned} &\overline{u'_i u'_j}^{(SGS)} = 2\nu_{SGS}S_{ij} - \frac{1}{3}\delta_{ij}\overline{u'_k u'_k}^{(SGS)} \\ &\nu_{SGS} = \left(C_s f_s \Delta_s\right)^2\sqrt{2S_{ij}S_{ij}} \end{aligned}\right\}, \tag{3}$$

where Smagorinsky constant C_s=0.1, filter scale $\Delta_s = \sqrt[3]{\Delta x \Delta y \Delta z}$, and f_s is damping function, $f_s = 1 - \exp\left(-y^+/25\right)$. Using these models, F_{ij} in Eq. (2) is modified as follows,

$$\left.\begin{aligned} &F_{ij} = -\delta_{ij}P - u_i u_j + 2\left(\nu + \nu_{SGS}\right)S_{ij} \\ &P = \frac{p}{\rho} + \frac{1}{3}\overline{u'_k u'_k}^{(SGS)} \end{aligned}\right\}. \tag{4}$$

These equations were solved by SMAC method. Spatial derivatives were approximated by second-order accuracy central finite difference on staggered grids. Uniform grids were applied in the streamwise and spanwise directions. In the wall-normal direction, grid points were concentrated in the near-wall region. Non-linear term and viscous term were treated explicitly, and pressure term and equation of continuity were treated implicitly. Second-order Adams-Bashforth method was applied for time marching. Poisson equation for pressure was solved using Fourier series expansions in the streamwise and spanwise directions together with tridiagonal matrix inversion.

The calculations were performed at Reynolds number based on friction velocity and channel width Re_τ of 1,300 (corresponding to Reynolds number of 27,000 based on centerline velocity and channel width). The flow was resolved using 128^3 grid points. The dimensions of calculation domain are $2.2H$ in the streamwise direction, H in the wall-normal direction and $0.74H$ in the spanwise direction. The grid spacing in the streamwise and spanwise directions was $\Delta x^+ = 22.5$ and $\Delta z^+ = 7.5$ in wall coordinates. That in the wall-normal direction was between $\Delta y^+_{\min} = 1.96$ (nearest the wall) and $\Delta y^+_{\max} = 19.6$ (at the channel center). The time increment used in our simulations was $\Delta t = 8.2\times10^{-6}$[sec] ($\Delta t^+ = 0.13$).

CALCULATION OF PARTICLE TRAJECTORIES

The particle motion for a small rigid sphere in a turbulent flow field is described by a complicated integrodifferential equation (Maxey & Riley, 1983). However, if the density of the particle is substantially larger than the density of the carrier fluid, the equation of particle motion can be simplified. The equation of the translational motion used in the simulations is given by,

$$m_p\frac{du_{pi}}{dt} = \frac{1}{2}\rho|\mathbf{u}_R|A\left[C_D u_{Ri} + C_{LR}\frac{\left(\mathbf{u}_R\times\boldsymbol{\omega}_R\right)_i}{|\boldsymbol{\omega}_R|}\right], \tag{5}$$
$$+ f_{LG}\delta_{i2} + m_p g\delta_{i1}$$

where m_p is particle mass, u_{pi} , particle velocity, C_D, drag coefficient, ρ, gas density, A, projected area of particle, C_{LR}, lift coefficient due to particle rotation, ω_{Ri}, particle rotational velocity, and u_{Ri} is gas velocity relative to the particle. The first term in the RHS of Eq. (5) expresses the drag force, the second term, the lift force due to rotational motion, f_{LG}, the lift force due to velocity gradient and g is acceleration of gravity. The empirical relation for C_D by Schiller & Nauman (1933) was employed,

$$C_D = \frac{24}{\mathrm{Re}_p}\left(1 + 0.15\,\mathrm{Re}_p^{0.687}\right), \tag{6}$$

where Re_p is the particle Reynolds number, $\mathrm{Re}_p = d_p|\mathbf{u}_R|/\nu$ (d_p: particle diameter, ν: kinematic viscosity of gas). Concerning the lift coefficient C_{LR} , a formula by Tanaka & Tsuji (1991) was used which was deduced from the experimental data by Maccoll (1928). For the lift force f_{LG} was employed only in the wall-normal component with Saffman's expression as follows (1965),

$$f_{LG} = -1.62 d_p^2 \rho u_{Rx}\sqrt{\nu\left|\frac{\partial u_{Rx}}{\partial y}\right|}\frac{\partial u_{Rx}/\partial y}{|\partial u_{Rx}/\partial y|}. \tag{7}$$

The equation of rotational motion is given by,

$$I\frac{d\omega_{pi}}{dt} = -C_T\frac{1}{2}\rho\left(\frac{d_p}{2}\right)^2|\boldsymbol{\omega}_R|\omega_{Ri}, \tag{8}$$

where I is the moment of particle inertia. The RHS of Eq. (8) is the viscous torque against the particle rotation, which is theoretically obtained by Dennis *et al.* (1980) and Takagi (1977). C_T is the non-dimensional coefficient determined by the

rotational Reynolds number, $\mathrm{Re}_R = d_p^2|\omega_R|/4\nu$.

NUMERICAL PROCEDURE

Initially, 4,800 particles were distributed uniformly in the calculation region. As the result, the particles were distributed various phases in the quasi-streamwise vortex. Fully developed state was used as the initial condition of gas flow field. Initial velocity and rotational velocity of particles were given the same values as those of the gas at each particle position. For the calculation of particle motion, the gas velocity at the particle position was given by 3-dimensional polynomial interpolation using values at eight grid-points surrounding the particle.

The gas flow in the raw flow field was solved with the high resolution grid points whose resolution is shown before. At each time step the gas velocity was filtered by cutting off high wave number components in the wave number space. The motion of particles which have the same initial conditions were calculated simultaneously in the raw flow field and filtered flow fields. We applied the 1-dimensional filtering in the streamwise and spanwise direction respectively. FFT was not available in the wall-normal direction due to the non-uniform grids, so that we did not apply the filtering in the wall-normal direction.

The particle position in a filtered flow field deviates from that in the raw flow field as the time increases. This deviation D in particle position at an instant was used as the measure of the effect of the filtering on the particle motion. In channel flows, statistical properties are functions of the distance from the wall y, so averages of D in each y-position which contains 400 particles were taken. We used six kinds of particles, the properties of which are the same as those in the experiments by Kulick *et al.*(1994) and Fessler *et al.* (1994), DNS by Rouson & Eaton (1994) and LES by Wang & Squires (1996). Table 1 shows the particle parameters. Stokes relaxation time τ_p shown in Table 1 was estimated by $\tau_p = \rho_p d_p/(18\mu)$ (ρ_p : particle density, μ : gas viscosity).

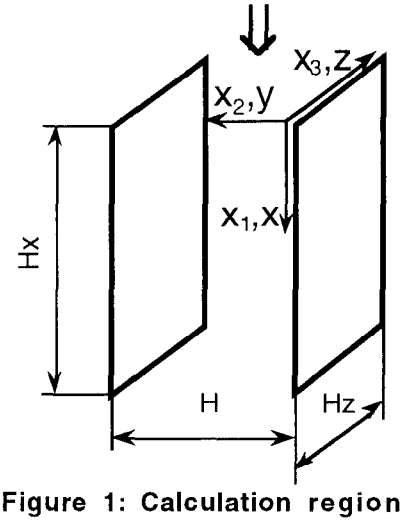

Figure 1: Calculation region

RESULTS

Figures 2~5 show the deviation of particle trajectories in the filtered fields from that in the raw flow field. The abscissas are wave length of cutoff filter scale λ_i^+ (i=x, z) and the ordinates are the deviation normalized by $\sqrt{\overline{u'_i{}^2}T}$, in which $\sqrt{\overline{u'_i{}^2}}$ is the gas turbulence intensity and T is the period of simulation. $\sqrt{\overline{u'_i{}^2}T}$ is supposed to be the characteristic length scale which represents the turbulent dispersion. The grid scale corresponds to half of the wave length. Figure 2 shows the effect of the cutoff wave length on the normalized deviation for the x-direction filter at the channel center (y_0^+=650, y_0^+ : initial y-position in wall unit), Figure 3 for the z-direction filter at the channel center, Figure 4 for the x-direction filter near the wall (y_0^+=110), Figure 5 for the z-direction filter near the wall in each component. These figures show that the particle motion is not affected by λ_i^+ in the region of small λ_i^+. This result means that the spatial resolution of LES is sufficient to resolve particle motion. When λ_i^+ becomes larger and exceed certain value, the deviation increases with increasing λ_i^+. Let the minimum wave length at which the deviation D can be neglected be $\lambda_{i\mathrm{cut}}^+$ (i=x, z). $\lambda_{i\mathrm{cut}}^+$ increases roughly with increasing St^+. From these figures, it is apparent that the lower the particle Stokes number, the larger the effect of small scale eddies on the particle motion. There are some plots showing that the magnitude of D is not correlated well with St^+ at large wave length. It may be because the time length in which D is examined is small compared with the time scale of the event of turbulence. It can be seen that there is some differences in the effect of filtering between the near -wall region and the channel center. The effect of filtering is more significant in the near-wall region than in the channel center.

To see the effect of filtering on the gas flow field the distributions of $(1/2)\omega_i^{+\prime}\,\omega_i^{+\prime}$ are shown in Figures 6 and 7. In these figures the streamwise direction corresponds to the horizontal direction and the spanwise direction corresponds to the vertical direction. The sizes of the area shown is 2880 in the streamwise direction and 960 in the spanwise direction in wall unit. It can be seen that the small scale fluctuation intensity is higher in the near-wall region than that in the channel center. Consequently the effect of filtering in the near-wall region is larger than that in the channel center. This tendency is consistent with the results in Figures 2~5.

It is difficult to define the critical cutoff wave length $\lambda_{i\mathrm{cut}}^+$ (i=x, z), because the deviation increases continuously with increasing λ_i^+. Therefore we defined $\lambda_{i\mathrm{cut}}^+$ as the cutoff wave length which gives 0.3% deviation. Figures 8 and 9 show $\lambda_{i\mathrm{cut}}^+$ versus stokes number for each initial y-position. These figures show that the spatial resolution in the z direction should be higher than in the x direction. $\lambda_{i\mathrm{cut}}^+$ increases with increasing St^+. The rate of increasing is remarked in the range of St^+>1000, and moderate in the range of St^+<1000. Here we make a simple

dimensional analysis based on Stokes number. Particle motion is affected by an eddy during the particle is contained in it. The time in which the particle is contained in the eddy is characterized by the eddy life time τ_e or the eddy crossing time τ_c. The smaller one dominates the phenomena. When the particle response time τ_p is smaller than those time scale τ_e or τ_c, the particle motion is affected by the eddy. In the critical case,

$$\frac{\tau_p}{\tau_c} \approx 1 \quad \text{(a) or} \quad \frac{\tau_p}{\tau_e} \approx 1 \quad \text{(b)}, \tag{9}$$

where $\tau_p = \rho_p d_p / (18\mu)$, $\tau_c = l_e / \overline{u_p}$, ($l_e$: length scale of the smallest eddy which can affect the particle motion, $\overline{u_p}$: mean particle velocity relative to the eddy), and $\tau_e \approx l_e^2 / \nu$. The eddy life time τ_e is estimated by assuming that kinetic energy of the eddy is dissipated by viscosity. Then, we assume that the critical cutoff wave length is given by $\lambda \approx l_e$, and $\overline{u_p} \approx \tau_p g$. The critical cutoff wave length λ is expressed by

$$\lambda \approx g\tau_p^2 \quad \text{(a) or} \quad \lambda \approx \sqrt{\nu \tau_p} \quad \text{(b)}, \tag{10}$$

or by a function of St^+ in wall unit,

$$\lambda^+ \approx \frac{g\nu}{u_\tau^3}\left(St^+\right)^2 \quad \text{(a) or} \quad \lambda^+ \approx \sqrt{St^+} \quad \text{(b)}. \tag{11}$$

In figures 8 and 9, lines by Eq.(11) are also shown. These lines are multiplied by coefficients and added by offsets so as to be fitted with numerical results. This offset wave length is derived by forgiving the 0.3% error in deciding critical cutoff wave length λ_{icut}^+. It is supposed that a trajectory of fluid particle (St=0) on the grids corresponding to the offset wave length differs in 0.3% from that on the grids which can resolve the smallest eddy. λ_{icut}^+ is given by Eq.(11a) in the region of large St^+ ($\tau_c < \tau_e$) and by Eq.(11b) in the region of small St^+ ($\tau_c > \tau_e$), divided on the point of intersecting these two lines. Equation (11) can express qualitative tendencies well.

In our previous simulations (Tanaka *et al.* 1997), the grid resolutions (Δx^+=45 and Δz^+=15, corresponding to wave length of λ_x^+=90 and λ_z^+=30 and St^+=300, 2110) are high enough to calculate the particle dispersion correctly within error of 0.3% to the characteristic length scale which represent the turbulent dispersion while t^+=100.

CONCLUSIONS

To determine the spatial resolution of LES which can resolve particle motion the effect of spatial resolution on the trajectories of particles was studied by using the filtered flow fields. The principal results are as follows;

(1) The minimum length scale of turbulent eddy affecting the particle motion increases with increasing particle Stokes number St^+. The rate of increasing is moderate at St^+ less than 1000 and large at St^+ more than 1000.

(2) The correlation between the particle Stokes number and the minimum length scale of turbulent eddy affecting the particle motion is obtained by a simple dimensional analysis based on the eddy-particle interactive time. The theoretical prediction agrees with the present numerical results qualitatively.

ACKNOWLEDGMENT

This work was supported in part by Grant-Aid for Scientific Research (No.09650188) of the Japanese Ministry of Education, Science and Culture.

REFERENCES

Dennis, S. C. R., Singh, S. N. & Ingham, D. B., The steady flow due to a rotating sphere at low and moderate Reynolds numbers, *J. Fluid Mech.*, **101**, (1980), 257-279.

Elghobashi, S. & Truesdell, G. C., Direct simulation of particle dispersion in a decaying isotropic turbulence., *J. Fluid Mech.*, **242**, (1992), 655-700.

Fessler, J. R., Kulick, J. D. & Eaton, J. K., Preferential concentration of heavy particles in a turbulent channel flow., *Phys. Fluids*, **6**(11), (1994), 3742-3749.

Gore, R. A. & Crowe, C. T., Effect of particle size on modulating turbulent intensity: Influence of radial location. *ASME/FED Turbulence Modifications in Dispersed Multiphase Flows*, (ed. E.E. Michaelides & D.E. Stock), **80**, (1989), 31-35.

Kulick, J. D., Fessler, J. R. & Eaton, J. K., Particle response and turbulence modification in fully developed channel flow., *J. Fluid Mech.*, **277**, (1994), 109-134.

Maccoll, J. H., Aerodynamics of a spinning sphere., *J. Roy. Aero Sci.*, **32**, (1928), 777-798.

Maxey, M. R. & Riley, J. J., Equation of motion for a small rigid sphere in nonuniform flow., *Phys. Fluids*, **26**, (1983), 883-889.

Rouson, D. W. I. & Eaton, J. K., Direct numerical simulation of turbulent channel flow with immersed particles., *ASME/FED Numerical Methods in Multiphase Flows* (ed. Sommerfeld, M.), **185**, (1994).

Saffman, P. G., The lift on a small sphere in a slow shear flow., *J. Fluid Mech.*, **22**, (1965), 385-400.

Schiller, L. & Nauman, A., *V. D. I. Zeits*, **77** (1933), 318.

Squires, D. K. & Eaton, J. K., Particle response and turbulence modification in isotropic turbulence., *Phys. Fluids*, A**2** (7), (1990), 1191-1203.

Takagi, H., Viscous flow induced by slow rotation of a sphere, *J. Phys. Soc. Japan*, 42, (1977), 319-325.

Tanaka, T. & Tsuji, Y., Numerical simulation of gas-solid two-phase flow in a vertical pipe: On the effect of inter-particle collision, *ASME/FED Gas-Solid Flows*, (1991), 123-128.

Tanaka, T., Yamamoto, Y., Potthoff, M. & Tsuji, T., LES of gas-particle turbulent channel flow, *Proceedings of the ASME Fluids Engineering Division Summer Meeting*, (1997), FEDSM97-3630(CD-ROM).

Wang, Q. & Squires, K. D., Large eddy simulation of particle-laden turbulent channel flow., *Phys. Fluids*, **8**(5), (1996), 1207-1223.

Table 1: Particle parameters

Material	Lycopodium		Glass			Copper
Density ρ_p [kg/m^3]	700		2500			8800
Diameter d_p [μm]	7	28	25	50	90	70
Stokes relaxation time τ_p [ms]	0.11	1.7	4.8	19	63	133
Terminal velocity v_t [m/s]	0.0010	0.016	0.046	0.18	0.47	0.93
$St = \tau_p / (H/u_\tau)$	0.0013	0.021	0.059	0.23	0.77	1.6
$St^+ = \tau_p / (\nu/u_\tau^2)$	2	27	76	301	998	2110

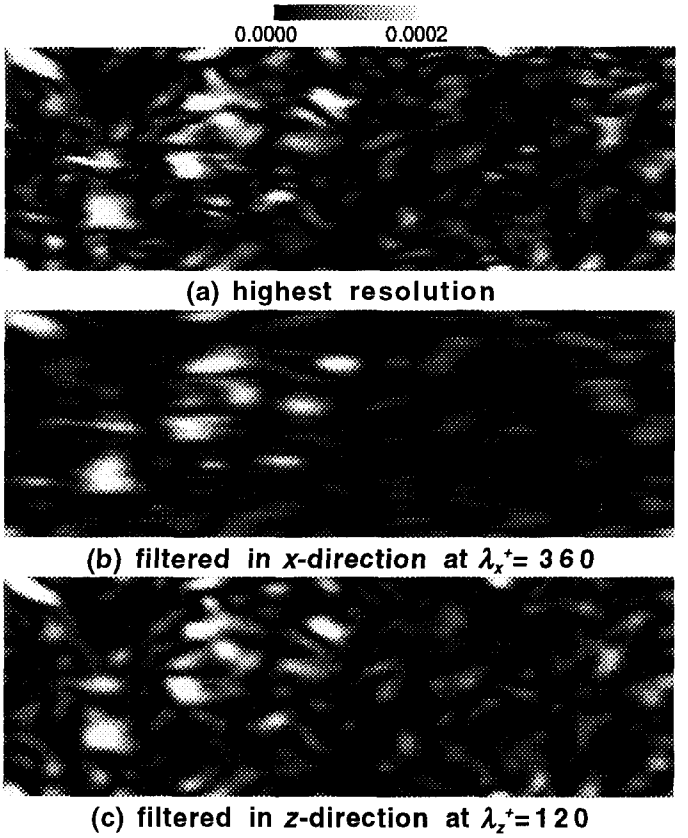

(a) highest resolution

(b) filtered in x-direction at $\lambda_x^+ = 360$

(c) filtered in z-direction at $\lambda_z^+ = 120$

Figure 6: Filtered fields, $(1/2)\omega_i^{+\prime}\omega_i^{+\prime}$ contour at the channel center plane ($y_0^+ = 650$)

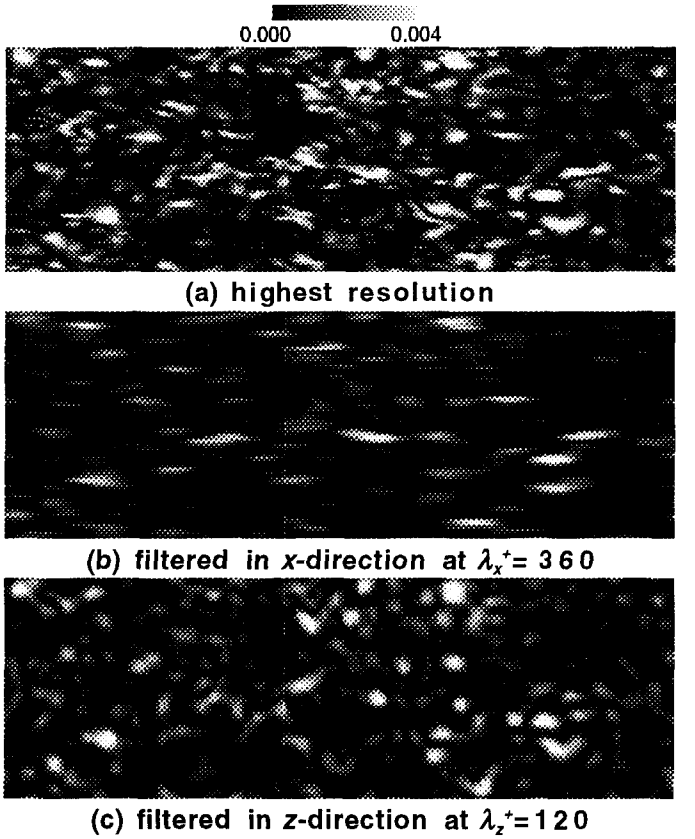

(a) highest resolution

(b) filtered in x-direction at $\lambda_x^+ = 360$

(c) filtered in z-direction at $\lambda_z^+ = 120$

Figure 7: Filtered fields, $(1/2)\omega_i^{+\prime}\omega_i^{+\prime}$ contour near the wall ($y_0^+ = 110$)

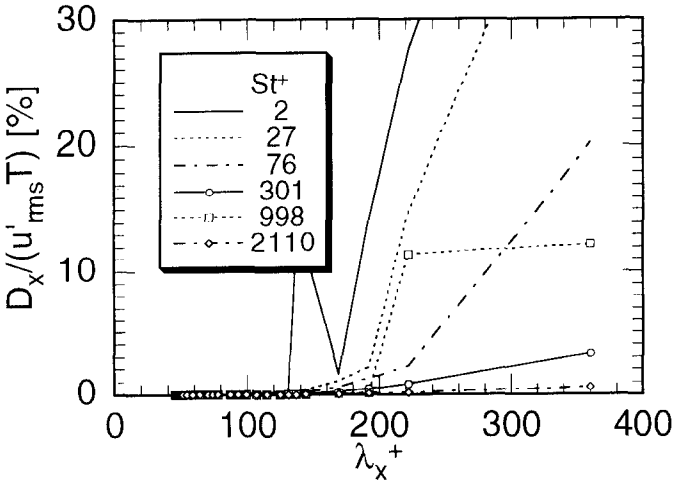

(a) *x*-component

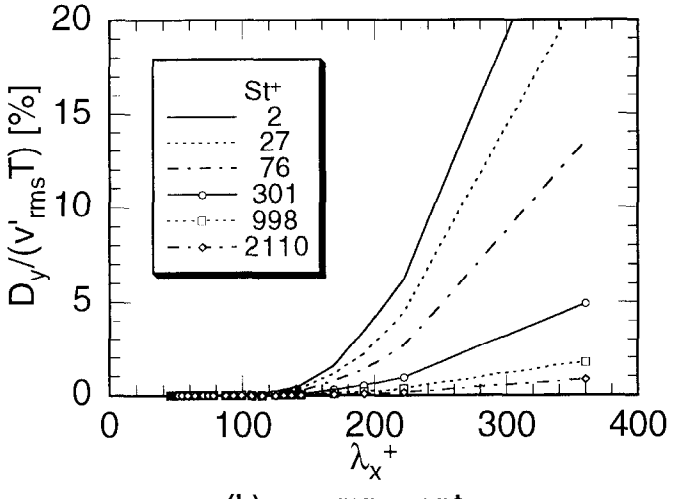

(b) *y*-component

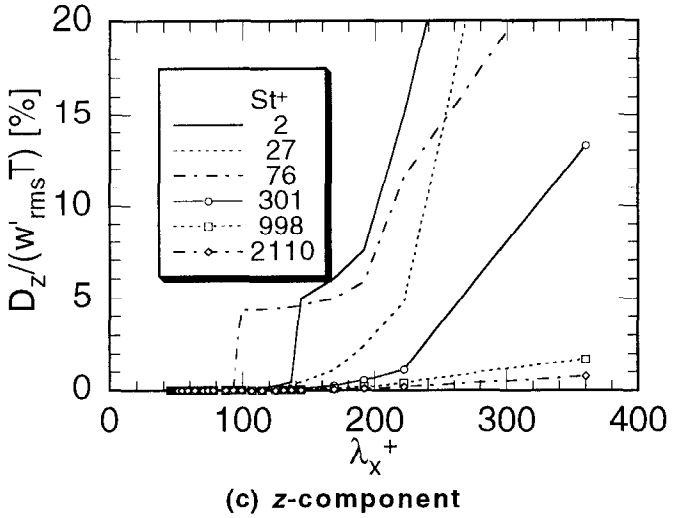

(c) *z*-component

Figure 2: Deviation by *x*-direction filter, $y_0^+=650$

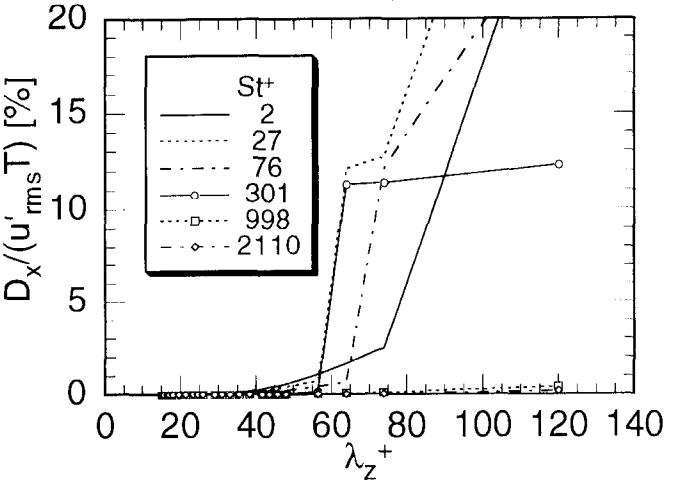

(a) *x*-component

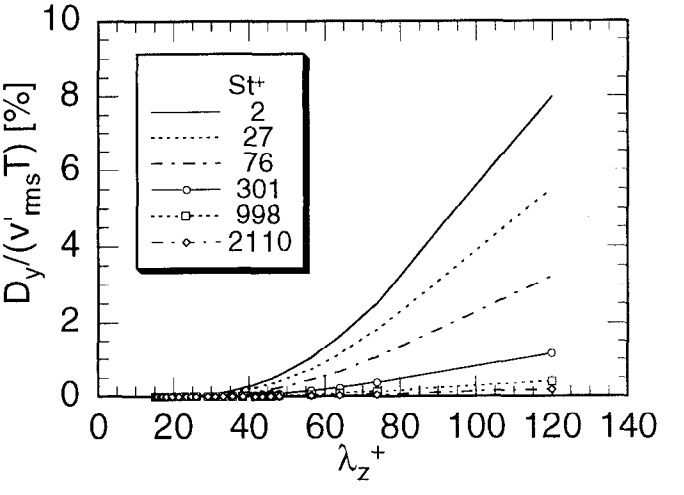

(b) *y*-component

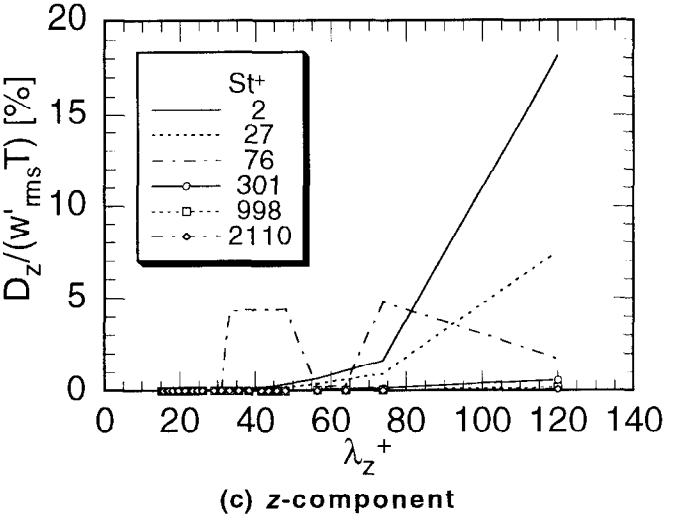

(c) *z*-component

Figure 3: Deviation by *z*-direction filter, $y_0^+=650$

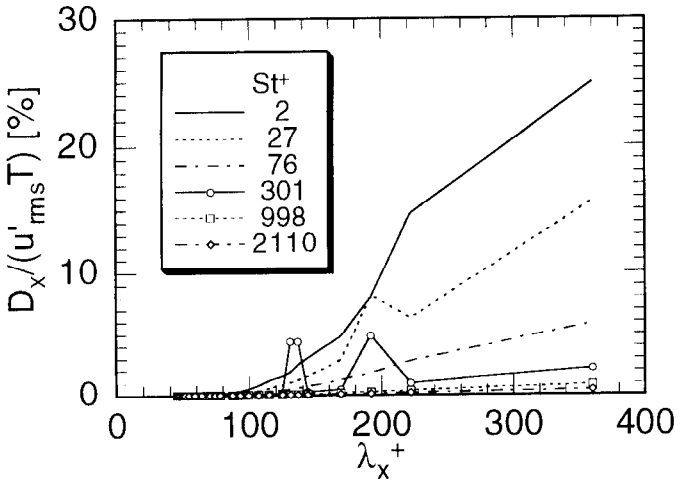

(a) *x*-component

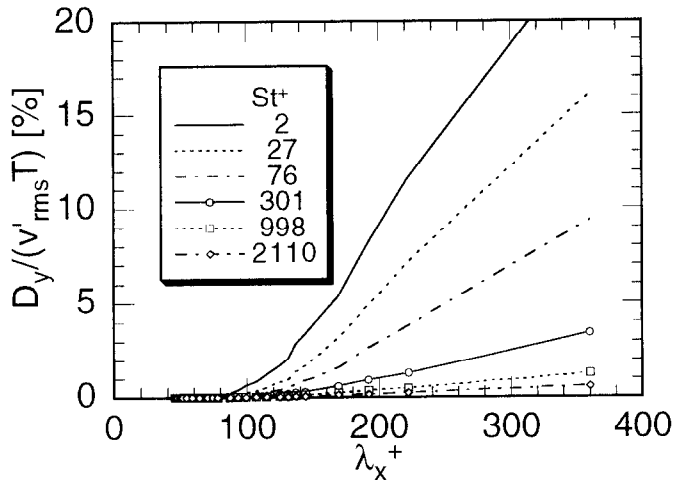

(b) *y*-component

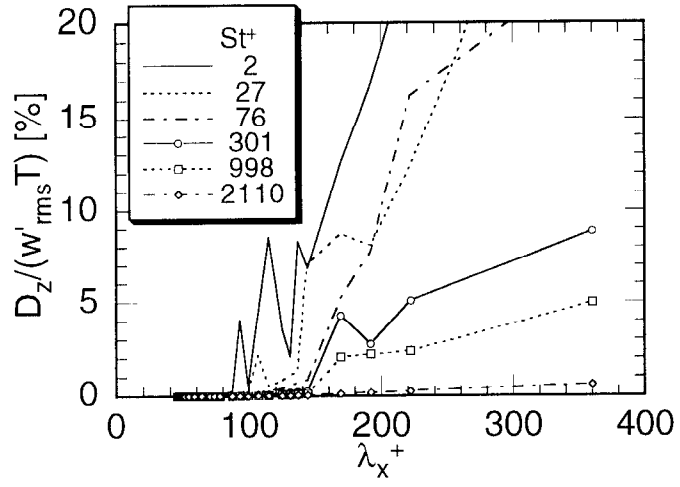

(c) *z*-component

Figure 4: Deviation by *x*-direction filter, $y_0^+=110$

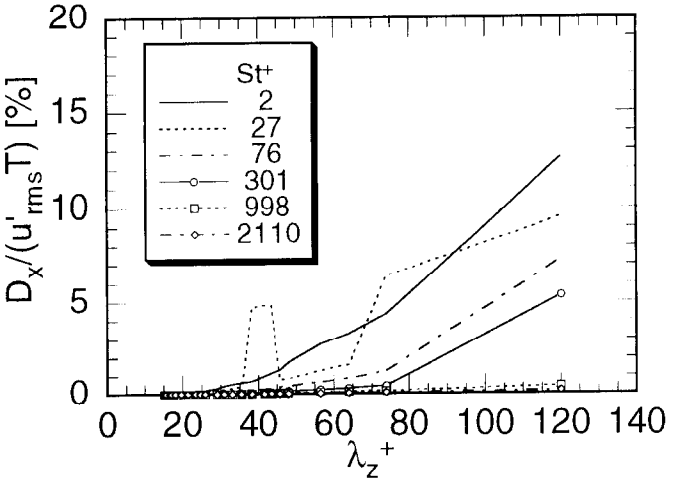

(a) *x*-component

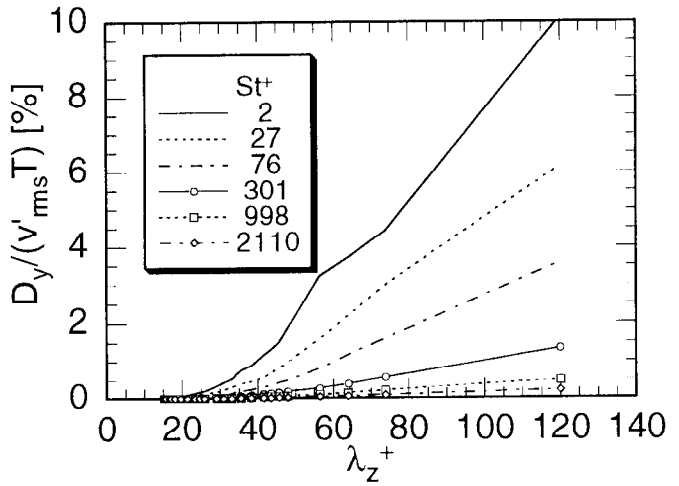

(b) *y*-component

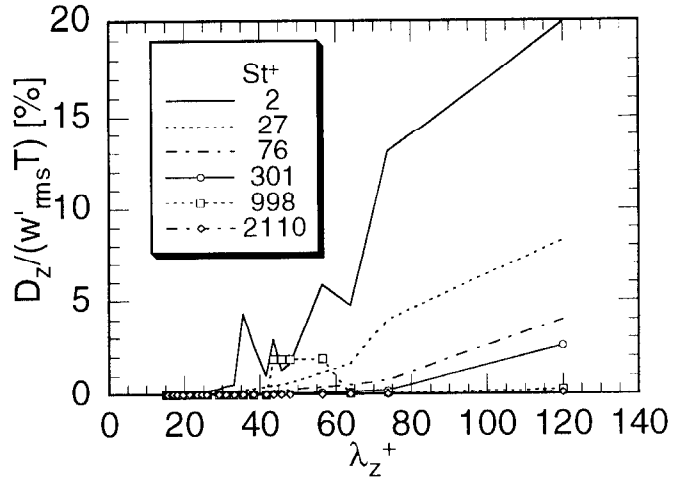

(c) *z*-component

Figure 5: Deviation by *z*-direction filter, $y_0^+=110$

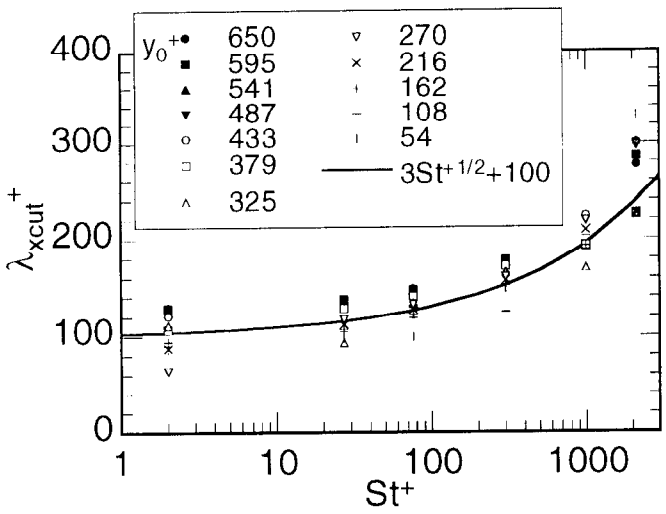

(a) *x*-component

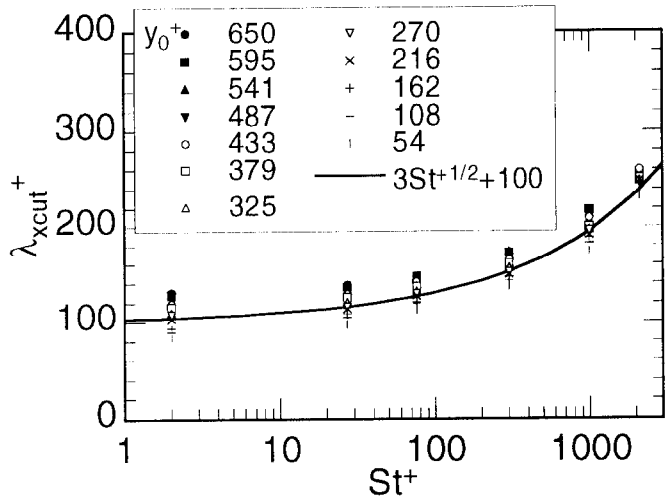

(b) *y*-component

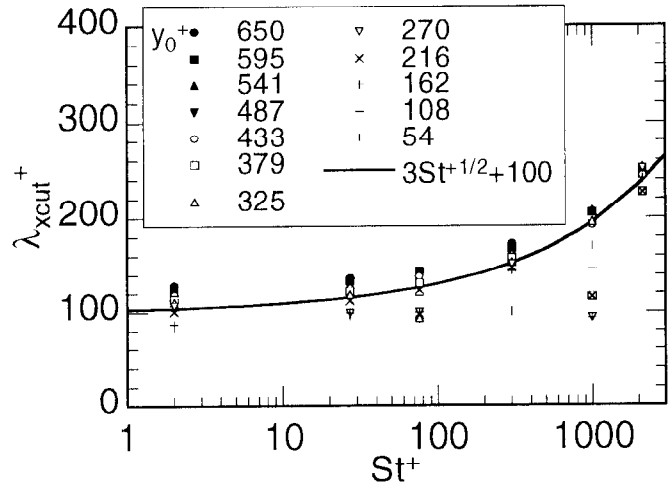

(c) *z*-component

Figure 8: Cutoff wave length at 0.3% deviation by *x*-direction filter

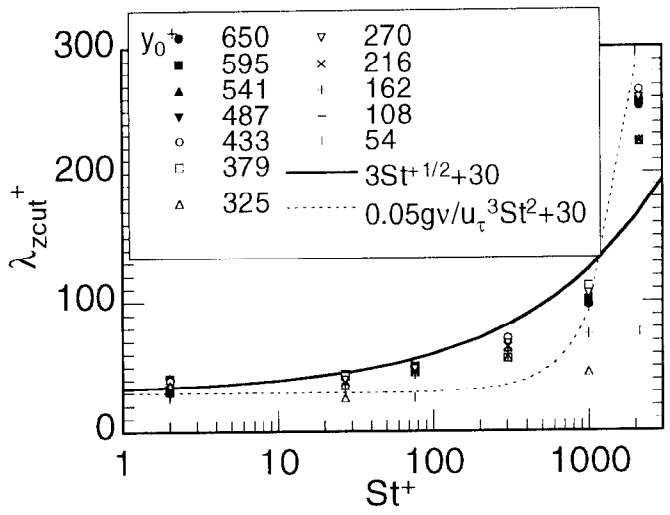

(a) *x*-component

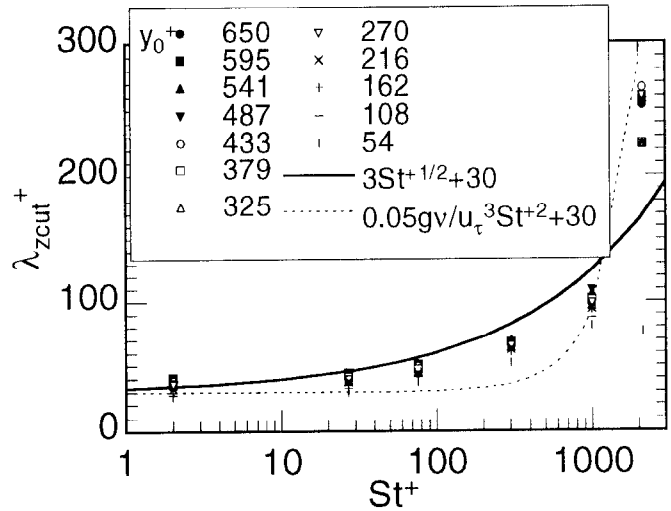

(b) *y*-component

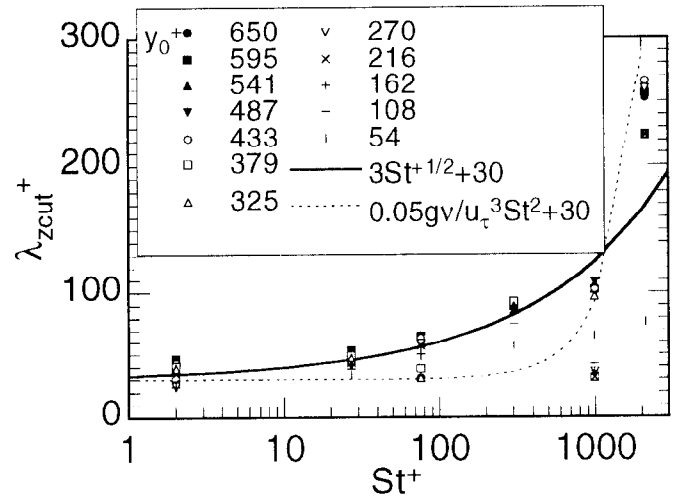

(c) *z*-component

Figure 9: Cutoff wave length at 0.3% deviation by *z*-direction filter